AGU PUBLICATIONS

Geophysical Research Letters

Supporting Information for

On the increase of climate sensitivity and cloud feedback with warming in the Community Atmosphere Models

Jiang Zhu[1,2*] and Christopher J. Poulsen[1]

[1]Department of Earth and Environmental Sciences, University of Michigan, Ann Arbor, MI 48109
[2]Climate and Global Dynamics Laboratory, National Center for Atmospheric Research, Boulder, CO 80305

Contents of this file

Text S1–S2
Figure S1–S2
Table S1–S3

Introduction

Supporting information includes text, table and figures to support the discussion in main article.

*Corresponding to: Jiang Zhu (jiangzhu@ucar.edu)

Text S1. Estimation of the contribution from λ_{cld} to ECS increases

We employ a bulk estimation method that has been used in previous studies (Gettelman et al., 2019; Gettelman, Kay, & Shell, 2012; Zelinka et al., 2020). To estimate the contribution from the cloud feedback to ECS changes, this method calculates a hypothetical ECS that would exist if the cloud feedback was changed but the radiative forcing and non-cloud feedbacks were kept unchanged. Specifically, ECSs for the climate states with two CO_2 levels in a model are expressed as

$$\mathrm{ECS}_1 = -\frac{F_1}{\lambda_{\mathrm{noncld},1}+\lambda_{\mathrm{cld},1}} \quad (1)$$

$$\mathrm{ECS}_2 = -\frac{F_2}{\lambda_{\mathrm{noncld},2}+\lambda_{\mathrm{cld},2}} \quad (2).$$

F is the radiative forcing of doubling CO_2, and $\lambda_{\mathrm{noncld}}$ and λ_{cld} are the "non-cloud" and the cloud feedback, respectively. The two background states are denoted using subscripts 1 and 2, respectively.

With values of ECS, F, and λ_{cld} for two climate states in each model, we first compute $\lambda_{\mathrm{noncld}}$ using equations (1–2). We next calculate hypothetical ECS_1' and ECS_2' due to the cloud feedback changes, as

$$\mathrm{ECS}_1' = -\frac{F_1}{\lambda_{\mathrm{noncld},1}+\lambda_{\mathrm{cld},2}} \quad (3)$$

$$\mathrm{ECS}_2' = -\frac{F_2}{\lambda_{\mathrm{noncld},2}+\lambda_{\mathrm{cld},1}} \quad (4).$$

Finally, the contribution of the cloud feedback to the ECS change is estimated as

$$\Delta\mathrm{ECS} = \frac{(\mathrm{ECS}_1'-\mathrm{ECS}_1)+(\mathrm{ECS}_2-\mathrm{ECS}_2')}{2} \quad (5).$$

The above estimation uses two-way calculations (forward in equation (3) and backward in equation (4)) to remove part of the dependence of ECS on the initial feedback parameter and forcing. CO_2 radiative forcing (F) are derived using the simplified equation in Byrne and Goldblatt (2014). Specifically, F are 3.9, 4.2, 4.6, and 5.4 W m^{-2} at 1, 2, 4, and 16× PIC, respectively. Results are expected to depend on the assumption of CO_2 radiative forcing but our major conclusion that climate feedbacks dominate the state dependence of

ECS still holds based on findings in previous studies (Colman and McAvaney, 2009; Meraner et al., 2013; Caballero and Huber, 2013; Zhu et al., 2019).

Using equations (1–5), we find that the cloud feedback approximately contributes 1.2–1.4 °C (> 70%) to the ECS increases in CAM versions (Table S2). Our results suggest that the non-cloud feedback does not change much in CAM6 (with a relatively narrower GMST and CO_2 range) and slightly decreases in CAM5 and CAM4 with warming (by <~0.1 W m^{-2} K^{-1}). These results are overall consistent with partial radiative perturbation analyses in previous Eocene simulations with a similar GMST range (Caballero & Huber, 2013; Zhu, Poulsen, & Tierney, 2019). Caballero and Huber (2013) show that the increase of water vapor feedback with warming is largely compensated by the associated decrease in the lapse-rate feedback in CCSM3 (their Figure 3B). Zhu et al. (2019) further suggest that the increase of the water vapor feedback with warming most likely results from the increase of the cloud feedback by comparing CESM1-CAM5 and CESM1-CAM4 simulations (their Figures 3B and S5).

Text S2. Additional cloud-controlling factors over the low-latitude subsidence regime

The subsidence strength (ω). Observational and large-eddy simulation-based studies (Bretherton, 2015; Myers & Norris, 2013) suggest that a stronger large-scale subsidence (ω) is associated with thinner and shallower clouds, favoring weaker cloud radiative effects ($\frac{\partial \mathrm{CRE}}{\partial \omega} > 0$). In response to CO_2-induced global warming, the tropospheric subsidence (ω at 700hPa) weakens in all CAM simulations ($\frac{d\omega}{d\mathrm{GMST}} < 0$; Figure S2a), forming a negative λ_{cld}. $\frac{d\omega}{d\mathrm{GMST}}$ is not a constant; it increases with GMST for the first CO_2 doubling in CAM 4, 5, and 6 (Figure S2b). This suggests that the sensitivity of large-scale dynamical response to global warming decreases with GMST, contributing to an increase of $\lambda_{\mathrm{cld\_subs}}$ with GMST. In contrast, our CAM5 and CAM6 simulations exhibit a decrease of shortwave $\lambda_{\mathrm{cld\_subs}}$ with GMST for the first CO_2 doubling (Figure 2m). Moreover, the increase of $\frac{d\omega}{d\mathrm{GMST}}$ with GMST appears to reach saturation when GMST exceeding ~20–23 °C, inconsistent with the large increases of $\lambda_{\mathrm{cld\_subs}}$ in CAM4 (Figure 2m). Overall, these results suggest that the large-scale dynamics is not a primary factor contributing to the $\lambda_{\mathrm{cld\_subs}}$ change with GMST.

The surface wind speed (U10). A decrease in lower wind speed (e.g. *U10*; wind speed at a reference height of 10 m) weakens the surface driven shear mixing and the associated latent heat flux, which thins low clouds ($\frac{\partial \mathrm{CRE}}{\partial U10} < 0$) (Bretherton, Blossey, & Jones, 2013). Our CAM simulations consistently show a decrease of wind speed with GMST ($\frac{dU10}{d\mathrm{GMST}} < 0$; Figure S2c), contributing to a positive $\lambda_{\mathrm{cld\_subs}}$. Magnitude of $\frac{dU10}{d\mathrm{GMST}}$ decreases with GMST, which appears to be a robust feature in almost all CAM simulations. Together, changes in wind speed contributes to a decrease of $\lambda_{\mathrm{cld\_subs}}$ with GMST. We suggest the mechanism of wind speed change is likely important for CAM6, especially when all the other cloud controlling factors act to increase CAM6 $\lambda_{\mathrm{cld\_subs}}$ with GMST (Figure 2,4 and Figure S2).

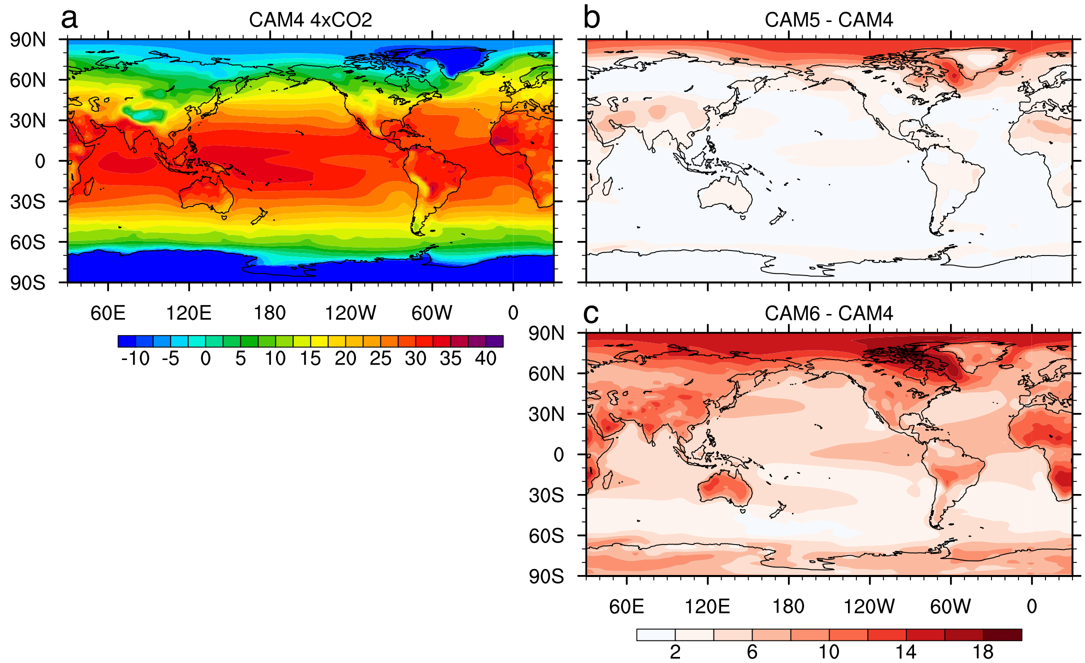

Figure S1. (**a**) Annual mean surface temperature in CAM4 SOM simulation with 4× PIC (units: °C). (**b**) Difference in surface temperature between CAM5 and CAM4 SOM simulations with 4× PIC (units: °C). (**c**) The same as (**b**), but for the surface temperature difference in CAM6.

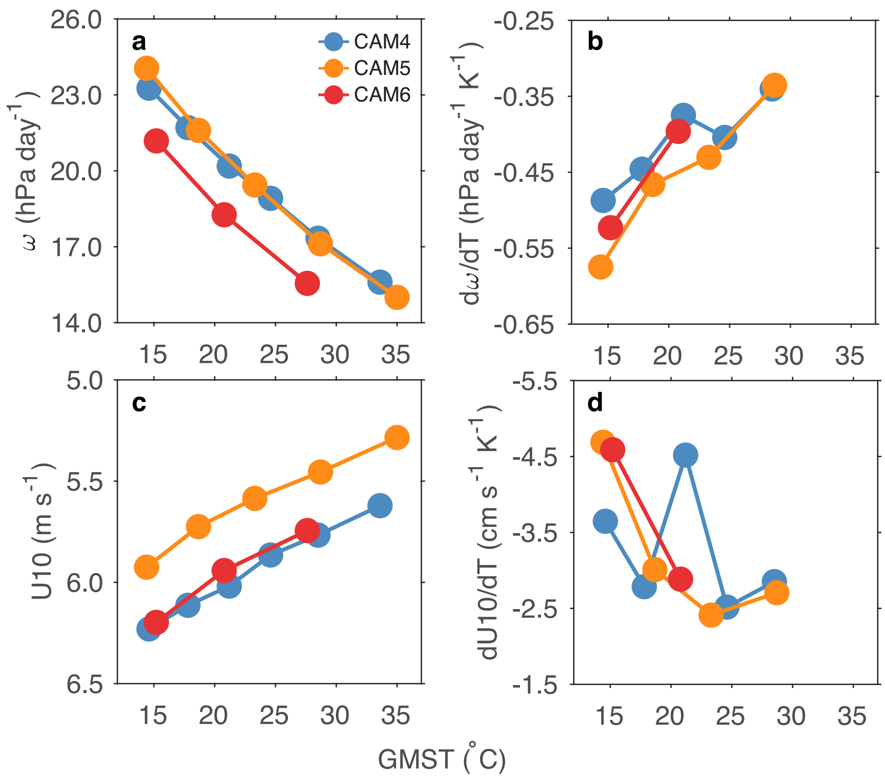

Figure S2. (**a**) ω at 700hPa averaged over the low-latitude subsidence regime as a function of GMST in the SOM simulations using CAM 4, 5, and 6. (**b**) The same as (**a**), but for the $\frac{\mathrm{d}\omega}{\mathrm{dGMST}}$, the sensitivity of ω to GMST changes. (**c**) and (**d**)The same as (**a**) and (**b**), but for the 10-m wind speed.

Table S1. λ_{cld} (units: W m^{-2} K^{-1}) diagnosed using PRP (first three columns) and APRP (last column, shortwave-only). PRP results are with the year-to-year standard deviation (n=10 in CAM4/5 and n=3 in CAM6). APRP decomposes shortwave λ_{cld} into contributions from cloud scattering, amount, and absorption. Scattering and amount feedbacks are shown in parentheses. Absorption changes little and is not shown. The standard deviation for APRP analysis ranges from 0.01 to 0.03 W m^{-2} K^{-1} and not listed.

		λ_{cld}	λ_{cld_LW}	λ_{cld_SW}	$\lambda_{cld\_SW\_APRP}$
CAM4	1× -> 2×	0.15±0.12	–0.02±0.05	0.16±0.10	0.11 (0.11, 0.11)
	2× -> 4×	--	--	--	0.29 (0.21, 0.19)
	4× -> 8×	0.21±0.07	0.04±0.04	0.18±0.07	0.12 (0.19, 0.04)
	8× -> 16×	--	--	--	0.30 (0.33, 0.09)
	16× -> 32×	0.37±0.05	–0.05±0.05	0.42±0.06	0.33 (0.38, 0.07)
CAM5	1× -> 2×	0.60±0.05	0.15±0.04	0.45±0.03	0.44 (0.06, 0.45)
	2× -> 4×	--	--	--	0.40 (0.09, 0.38)
	4× -> 8×	0.78±0.04	0.21±0.03	0.57±0.04	0.53 (0.26, 0.36)
	8× -> 12×	1.04±0.02	0.26±0.05	0.79±0.04	0.75 (0.44, 0.40)
CAM6	1× -> 2×	0.97±0.03	0.22±0.04	0.76±0.05	0.79 (0.32, 0.55)
	2× -> 4×	1.07±0.02	0.21±0.03	0.86±0.04	0.88 (0.46, 0.51)

Table S2. Calculation of ECS changes (ΔECS) that are attributed to the cloud feedback increases in CAM 4, 5, and 6. In each model, ECS (°C), the cloud and non-cloud feedbacks (λ_c and λ_{nc}; W m^{-2} K^{-1}), and CO_2 radiative forcing (F; W m^{-2}) from two climate states with the lowest and highest possible CO_2 levels were used. Note the large uncertainty in CAM4 λ_c at the 1×CO_2 level (see also Table S1).

	ECS_1	$\lambda_{c,1}$	F_1	$\lambda_{nc,1}$	ECS_2	$\lambda_{c,2}$	F_2	$\lambda_{nc,2}$	ΔECS
CAM6 (1, 2×)	5.5	0.97	3.9	–1.67	6.9	1.07	4.2	–1.69	0.9 (70%)
CAM5 (1, 4×)	4.2	0.60	3.9	–1.52	5.4	0.79	4.6	–1.65	1.0 (90%)
CAM4 (1, 16×)	3.2	0.15	3.9	–1.36	5.1	0.37	5.4	–1.42	0.8 (40%)

Table S3. Fraction area coverage (unitless) of the low-latitude subsidence and ascending regimes in CAM 4, 5, and 6 simulations. Fraction of the high-latitude cloud regime is invariant (0.47). CAM4 results include simulations with 1, 2, 4, 8, 16, and 32× PIC. CAM5 results include 1, 2, 4, 8, and 12× PIC. CAM6 results include 1, 2, and 4× PIC.

		1×	2×	4×	8×	16× or 12×	32×
CAM4	low - subs.	0.33	0.33	0.33	0.32	0.33	0.34
	low - asce.	0.20	0.21	0.21	0.21	0.20	0.19
CAM5	low - subs.	0.33	0.32	0.31	0.31	0.32	--
	low - asce.	0.20	0.21	0.22	0.22	0.21	--
CAM6	low - subs.	0.34	0.33	0.33	--	--	--
	low - asce.	0.20	0.20	0.20	--	--	--